A deterministic approach for predicting the transformation of starch suspensions in tubular heat exchangers

Artemio Plana-Fattori, Denis Flick, Fabrice Ducept, Christophe Doursat, Camille Michon, Samir Mezdour

A deterministic approach for predicting the transformation of starch suspensions in tubular heat exchangers

A. Plana-Fattori[1,2,#],
D. Flick[1,2],
F. Ducept[1,2],
C. Doursat[1,2],
C. Michon[1,2],
S. Mezdour[1,2]

1) AgroParisTech, UMR1145 Ingénierie Procédés Aliments, F-75231 Paris, France
2) INRA, UMR1145 Ingénierie Procédés Aliments, F-91300 Massy, France

Corresponding author address:
Artemio Plana-Fattori, AgroParisTech, 16 rue Claude Bernard, 75231 Paris, France;
e-mail: artemio.planafattori@agroparistech.fr

Abstract

Numerical modeling of fluid flow, heat transfer and transformation is conducted for an aqueous suspension of starch granules running throughout a four-heating-section tubular exchanger. The numerical model considers the transformation kinetics and the rheological behavior of the starch suspension as determined from laboratory work; further, the model includes the geometrical characteristics of the heat exchanger, as well as the operating conditions which were considered in running it. Model predictions are compared with results from experimental work, after sampling the starch suspension under thermal processing and later characterizing it using laboratory techniques. The numerical model predicts the bulk swelling state of the starch suspension at a level of agreement (–41 % in volume mean diameter increase) which is better than the one reached after assuming plug-flow and radially-independent temperature (–66 %). The inclusion of two-way coupling between the relevant phenomena constitutes therefore a positive improvement.

1. Introduction

Manufacturing food products in a reproducible manner requires understanding the mechanisms which drive the transformation of the ingredients along the processing pathway. For instance, in dairy desserts the milk is mixed with starch, to which carrageenan is added as a gelling agent (Doublier and Durand, 2008). Experimental work at laboratory scale has been conducted in order to study the influence of thermal treatment on the structure of whey proteins (Tolkach and Kulozik, 2007; Nicolai et al., 2011), of starch granules (Ratnayake and Jackson, 2008; Liu et al., 2009; Schirmer et al., 2013) and of carrageenan chains (Piculell, 2006; Nunez-Santiago et al., 2011). The interactions occurring between these ingredients have been studied and, for a variety of blends, the rheological behavior was analyzed along the batch thermal history (Verbeken et al., 2006; Doublier and Durand, 2008; Noisuwan et al., 2009; Huc et al., 2014; Matignon et al., 2014a, 2014b, 2015). The preparation of dairy desserts at industrial scale includes, among other steps, thermal processing under continuous flow. The phenomena of fluid flow, heat transfer and product transformation are strongly coupled within heat exchangers: transformation affects the characteristics of the product (e.g., particle sizes), with consequences on its rheological behavior and hence on the velocity field inside the processing unit. In turn, fluid flow influences heat transfer while the temperature level drives the transformation rate. As a consequence, the final structure of the liquid product can depend not only on the interactions between the ingredients but also on the geometry and on the thermal and dynamical operating conditions associated with the heat exchanger.

To predict the transformation of a liquid food product along its thermo-dynamical history is a challenging task. Physics-based and observation-based modeling approaches constitute complementary tools for food product, processes, and equipment designers. Physics-based models especially can provide a level of insight that is often not possible

58 experimentally (Datta, 2008). The phenomena of fluid flow, heat transfer, and product
59 transformation need to be considered in the case of the thermal processing of liquid food
60 products under continuous flow. The rheological behavior of liquid food products is typically
61 non-Newtonian and temperature-dependent; therefore, it is difficult to derive analytical
62 solutions for the conservation equations of mass, momentum and energy.

63 Computational Fluid Dynamics (CFD) has been employed to study a number of
64 problems in food engineering and related disciplines (Norton and Sun, 2006; Galeazzo et al.,
65 2006; Lemus-Mondaca et al., 2011; Khatir et al., 2013; Norton et al., 2013; Rocha et al.,
66 2013; Defraeye, 2014). However, limited efforts were devoted to coupled problems involving
67 liquid food products whose rheological behavior evolves as the transformation progresses
68 along the processing pathway. Bouvier et al. (2014) studied the thermal denaturation-
69 aggregation of whey proteins flowing under turbulent flow in a plate heat exchanger; those
70 authors obtained promising agreement between model predictions and observations of the
71 transformation state reached by the liquid product, after assuming a simple rheological
72 behavior for the whey protein solutions under consideration (Newtonian, temperature-
73 dependent). Liao et al. (2000) considered a more complex rheological behavior and developed
74 a numerical model coupling fluid flow, heat transfer and gelatinization of waxy rice starch
75 paste; the apparent viscosity of the product was described through a power law, and both the
76 consistency coefficient and the behavior index were assumed to be temperature-dependent.
77 We can argue that describing the rheological behavior as a function of the local temperature is
78 not a robust strategy. It can be shown that the characteristics of the liquid product, and hence
79 its rheological behavior at a given position in the heat exchanger, depend not only on the local
80 conditions but also on the thermal (and eventually dynamical) histories associated with the
81 fluid parcels running at this position (Chantoiseau et al., 2012; Plana-Fattori et al., 2013). The
82 two-way coupling between product transformation, fluid flow and heat transfer phenomena

via the rheological behavior constitutes a robust strategy for predicting the transformation of a liquid product along its thermo-dynamical history.

In the logical continuation of previous efforts (Plana-Fattori et al., 2013), this study presents a numerical model for predicting the transformation of a starch suspension running throughout an existing four-heating-section tubular exchanger. We focus on a given starch suspension (type and concentration), and the parameters relevant to the numerical model are estimated through our own experimental protocol at laboratory scale. Both the swelling kinetics and the rheological behavior are represented more realistically than in that previous study; on the one hand, a threshold temperature is assumed for the swelling kinetics rate (rather than an Arrhenius-like approximation); on the other hand, the progressive shear-thinning behavior of the starch suspension is described. Later, we compare model predictions of the swelling state reached by the suspension, with observations obtained at pilot scale by running the tubular heat exchanger whose geometry and operating conditions are considered in the numerical model. The objective of this study was double: firstly to implement the coupled model for thermal processing at pilot scale by applying key model parameters obtained from experimental work at laboratory scale, and secondly to assess the improvement that this coupled model represents relatively to a simpler approach, based on the assumption of plug-flow and radially-independent temperatures. Results constitute a meaningful step towards the implementation of numerical models able to represent the variety of dynamical and thermal conditions experienced by realistic food fluid parcels during their pathway in the processing unit. They will be useful for the design of starch suspension thermo-mechanical treatments.

2. Coupled physical problem

We are interested in the phenomena of fluid flow, heat transfer and liquid product

transformation occurring within a tubular heat exchanger which is running under stationary conditions. Conservation equations for mass, momentum and energy can be expressed as:

$$\vec{\nabla}.\left(\rho\,\vec{u}\right)=0 \tag{1}$$

$$\rho\left(\vec{u}\cdot\vec{\nabla}\right)\vec{u}=\vec{\nabla}\cdot\left(-p\,\vec{I}+\eta\left(\vec{\nabla}\vec{u}+\left(\vec{\nabla}\vec{u}\right)^{T}\right)-\frac{2}{3}\eta\left(\vec{\nabla}\cdot\vec{u}\right)\vec{I}\right) \tag{2}$$

$$\rho C_P\left(\vec{u}\cdot\vec{\nabla}\right)T=\vec{\nabla}\cdot\left(\lambda\,\vec{\nabla}T\right) \tag{3}$$

where $\vec{u}$ is the velocity (magnitude in m/s), p is the pressure (Pa), T is the temperature (K); ρ is the product's density (kg.m^{-3}), η its apparent viscosity (Pa.s), C_P its specific heat capacity (J.kg^{-1}.K^{-1}), and λ its thermal conductivity (W.m^{-1}.K^{-1}).

In this exploratory study focus is on the transformation of an aqueous suspension of chemically-modified waxy maize starch. Under heating, this liquid product undergoes a quite simple transformation: starch granules swell without either rupture of swollen granules or release of soluble species in water (Matignon et al., 2015). Hence, the volume occupied by the granules can indicate the transformation state regarding its influence on the apparent viscosity of the starch suspension. At a given time in the thermal history of a suspension droplet, the solid volume fraction Φ can be estimated as:

$$\Phi=\Phi_0\left(D/D_0\right)^3 \tag{4}$$

where D (µm) is the volume mean diameter of starch granules; values D_0 and Φ_0 correspond to the condition of untreated starch, before any thermal treatment. The transformation state associated with the starch suspension can also be indicated by the dimensionless value of the volume mean diameter (also known as swelling degree, S):

$$S=\left(D-D_0\right)/\left(D_{MAX}-D_0\right) \tag{5}$$

where D_{MAX} is the volume mean diameter after the maximum thermal treatment here considered.. In the case of a modified waxy starch suspension in water, the variation in the

swelling degree over time can be described using a second-order kinetics equation (Lagarrigue et al., 2008):

$$\frac{dS}{dt} = V\{T\}(1-S)^2 \quad (6)$$

where V is the temperature-dependent swelling kinetics rate (s^{-1}). Equations (4, 5, 6) summarize the product swelling for a travelling droplet in the starch suspension. The following conservation equation puts in evidence the inherent coupling which occurs between starch swelling, fluid flow and heat transfer at every position of the processing unit:

$$\vec{u} \cdot \vec{\nabla} S = V\{T\}(1-S)^2 + \vec{\nabla} \cdot \left(d_S \, \vec{\nabla} S \right) \quad (7)$$

where d_S is a diffusion coefficient ($m^2.s^{-1}$). Equation (7) states that the swelling state results from a) convective transport, b) temperature-dependent swelling of starch granules, and c) diffusion around the position under consideration. The coefficient d_S considered in this equation expresses the Brownian (random) diffusion affecting the starch granules in the suspension as well as some diffusion between parallel pathways along the exchanger.

Governing equations (1, 2, 3, 7) are solved in this study with the help of numerical modeling tools throughout a sequence of computational domains, as summarized in Section 4. The first step of our modeling approach is the description of the transformation kinetics and the rheological behavior of the liquid product as functions of the state variables.

3. Estimation of model parameters

3.1. Experimental work

The liquid product is a 3.42 % w/w starch suspension in water. Chemically-stabilized and cross-linked waxy maize starch (acetylated adipate distarch, C*Tex 06205) was kindly supplied by Cargill (Baupte, France). It consisted of at least 99 % of amylopectin and a maximum of 0.4 % w/w of endogenous proteins. The product was prepared by adding the

155 starch powder to a 0.1 M NaCl aqueous solution. Before any thermal treatment, the resulting
156 liquid remained at 50 °C for 30 minutes under continuous gentle stirring. Test tubes of 50 mL
157 were used to ensure an equivalent thermal history for all the fluid parcels contained in the
158 sample, while being large enough to enable further analyses. Stirring was performed with a
159 magnetized bar under permanent rotation (500 rpm) inside the test tube.

160 Thermal treatments consisted of a heating and a cooling step, both under continuous
161 stirring. The role of the cooling step was to stop product transformation as rapidly as possible
162 in order to associate different "heating times" with their corresponding "swelling states". The
163 heating step started when the product sample was removed from the 50 °C water bath and
164 immersed immediately in the second water bath, which was maintained at 90 °C. The cooling
165 step started when the sample was removed from the hot water bath and immersed
166 immediately in the third water bath, maintained at about 4 °C. The product's temperature was
167 initially between 62 and 92 °C (depending on heating duration) and then rapidly fell. The
168 cooling step was halted when the temperature reached 10 °C.

169 The product's temperature was recorded every 15 seconds during the whole heating
170 and cooling steps. The choices regarding the temperature in the hot water bath (90 °C) and the
171 heating duration (up to 64 minutes) enabled significant changes in the particle size
172 distribution and apparent viscosity. Temperatures close to 90 °C are involved in industrial
173 starch processing (see for instance Thomas and Atwell, 1999).

174 Figure 1A summarizes the thermal history obtained after each test: starting at 50 +/–
175 0.2 °C, the product's temperature firstly increased during the prescribed heating time and then
176 decreased during the cooling step. Tests are labeled in terms of heating time duration.

177 The particle size distribution associated with each sample was measured using a
178 Malvern Mastersizer 2000 laser granulometer (Malvern Instruments Ltd, United Kingdom)
179 equipped with a 300 mm Fourier cell (range: 0.05–879 μm). Drops of product were placed in

180 the cell (100 mL) until obscuration reached about 20 %, corresponding to a dilution of 1/100.
181 Typical values were assumed for the real and imaginary parts of the refractive index of starch
182 granules (1.53 and 0.01; Nayouf et al., 2003). Samples were analyzed twice within less than
183 15 minutes at room temperature, and the volume mean diameter was retained for further
184 application. For a given sample, the two estimates of the volume mean diameter were always
185 closer than 0.5 µm.

186 Rheological measurements were performed using a MCR 301 rheometer (Anton Paar,
187 Austria) equipped with coaxial cylinders. The temperature was controlled with a Peltier
188 system. The flow behavior of the suspension was measured at 20 °C. Increasing and
189 decreasing shear scans were performed stepwise following a logarithmic scale, firstly from 1
190 to 500 s^{-1} and then from 500 to 1 s^{-1}. Each shear scan was performed twice, and the whole
191 sequence took less than 15 minutes. The range 1 to 500 s^{-1} includes the maximum shear rate
192 expected at the heat exchanger.

193

194 *3.2. Kinetics parameters*

195 Figure 1B presents the volume mean diameter as a function of the heating time. This
196 display offers evidence that the first four minutes of heating play a major role in driving the
197 swelling state of the starch suspension. Between 1 and 8 min of heating, replicating a test
198 associated with a given heating time can allow volume mean diameters differing by some
199 micrometers. After 64 minutes of heating, the replicates agreed by better than 1 °C in
200 temperature and better than 0.5 µm in volume mean diameter.

201 The influence of temperature on the swelling kinetics rate is a challenging issue when
202 it comes to representing the transformation of starch suspensions under heating. Indeed, as
203 revealed by studies performed since the 1940s, starch granules can suddenly increase many
204 times in size within a small range of temperature at about 65 °C while the viscosity of the

suspension also increases rapidly (Freund, 1944). Such a sudden influence of temperature on the swelling kinetics rate can be approximated by:

$$V\{T\} = 0 \quad \text{if} \quad T < Ta, \tag{8a}$$

$$V\{T\} = Va\,(T - Ta) \quad \text{if} \quad T > Ta, \tag{8b}$$

where Ta is a threshold temperature and Va is a constant value ($s^{-1}.°C^{-1}$). Recent observations have shown that the changes in starch granule size become significant above a certain temperature (e.g. Malumba et al., 2013); from this perspective, equations (8) constitute a first-order approximation for such a change in the swelling kinetics rate.

The volume mean diameter D after a given time t depends on the whole thermal history of the sample, since the beginning of the thermal treatment (integration of equation 6):

$$D\{t\} = D_0 + (D_{MAX} - D_0)(1 - 1/(1 + X\{t\})) \tag{9a}$$

$$X\{t\} = \int_0^t V\{T\{t'\}\}\,dt' \tag{9b}$$

where $V\{T\{t'\}\}$ is estimated through equation (8) for temperature T at time t'. Equations (9) can be used to estimate the parameters Va and Ta, after exposing the starch suspension to a number of thermal treatments.

All the available tests are shown in Figure 1. Parameters Va and Ta were estimated from tests corresponding to the heating times of 1 min (three replicates), 1.5 min, 2 min (three replicates), 4 min (two replicates) and 8 min. Sample temperatures corresponding to these five heating times were about 62, 70, 72, 83, and 89 °C respectively. Tests corresponding to the heating times of zero (no hot bath) and 64 minutes allowed assessing the extreme values D_0 = 16.3 µm and D_{MAX} = 43.3 µm. The values for parameters Va and Ta were estimated by minimizing the sum of squared deviations between the experimental values of D and those calculated from equation (9), considering their respective thermal histories; we obtained Ta = 61.1 °C and Va = 3.79 10^{-3} $s^{-1}.°C^{-1}$.

Figures 1B and 1C compare volume mean diameter values obtained from experiment and predicted through equation (9), assuming the longest thermal history (heating time 64 min). Predictions agreed with experiment by better than 3 µm, and often better than 1 µm. The averaged relative error between predictions and experimental values is about 6 % for heating times from 0 to 64 minutes.

It must be noted that the swelling kinetics described by equations (6) and (8) is empirical; these equations describe how the thermal history of suspension droplets can be translated into changes affecting the volume mean diameter of the starch suspension as seen through laser granulometry. No attempt was made to study the heat and mass transfers occurring between starch granules and the surrounding water. We can anyway estimate the heat penetration time from granule surface down to the center, by considering typical values for the thermal diffusivity of starch (about $2\ 10^{-7}$ m^2/s; see for instance Rodriguez and de la Cruz, 2003). The result obtained (a few milliseconds) is four orders of magnitude smaller than the mean residence time of the starch suspension in the heat exchanger considered (about 50 seconds). Therefore, we can assume that starch granules exhibit a uniform temperature, and that it varies during their pathway throughout the heat exchanger in the same manner as the surrounding water temperature.

3.3. Rheological parameters

Figure 2 shows the apparent viscosities of pasted starch suspensions gathered through Couette rheometry at 20 °C. These measurements were obtained after the tests corresponding to heating times of zero (no hot bath), 1, 2, 4 and 8 minutes. The starch suspension became shear-thinning as granule swelling progressed, suggesting describing the apparent viscosity through an Ostwald power law with a flow behavior index depending on the swelling state. In addition, the apparent viscosity increased with the heating time, suggesting that the

consistency coefficient can be expressed as a function of the swelling state too. Finally, as a consequence of the relatively low mass concentration of starch in the suspension (3.42 %), the apparent viscosity at a given swelling state is expected to decrease with the local temperature, following a behavior similar to that exhibited by pure water.

The apparent viscosity associated with the starch suspension is hereinafter described using the following approximations:

$$\eta\{\dot{\gamma}, \Phi, T\} = K\{\Phi, T\}\dot{\gamma}^{n\{\Phi\}-1} \tag{10a}$$

$$K\{\Phi, T\} = k_1 \exp(k_2 \Phi)\, \eta_{water}\{T\} \tag{10b}$$

$$n\{\Phi\} = n* + (1-n*)\exp(-k_3 (\Phi - \Phi_0)) \tag{10c}$$

where K is the consistency coefficient (Pa.s^n), n is the flow behavior index, $\dot{\gamma}$ is the shear rate (s^{-1}) and η_{water} is the dynamic viscosity associated with pure water (Pa.s). Equation (10c) expresses that the flow behavior index exhibits an asymptotic pattern towards the value $n*$ as the solid volume fraction increases. Equations (10) express the mean dependence of the apparent viscosity with the shear rate, the solid volume fraction, and the temperature, while requiring only few parameters. More-detailed descriptions could reconcile the Newtonian plateau and the shear-thinning behavior (see for instance the grey squares in Figure 2); however, such an improvement would require a higher number of parameters.

The parameters required by equation (10) were estimated from the experimental values shown in Figure 2. Best fit values were estimated by minimizing the sum of squared deviations between the predictions and experimental values of apparent viscosity; we obtained k_1 = 0.662 s^{n-1}, k_2 = 13.6, k_3 = 4.91 and $n*$ = 0.55. Lines in Figure 2 indicate the predictions of the apparent viscosities corresponding to the five thermal treatments; the averaged relative error between predictions and experimental values is about 17 %.

It must be noted that the rheological behavior described by equations (10a) to (10c) is

empirical, with no considerations on the changes affecting starch granules under thermal treatment. Equations (10a) to (10c) associate the apparent viscosity of the starch suspension and the volume mean diameter of starch granules provided by Couette rheometry and laser granulometry respectively; changes in size are explicitly described via the volume mean diameter, while changes in other starch granules' characteristics (like shape and deformability) are implicitly accounted for in the mean general behavior described through equations (10) by modifying the values of constants k1, k2 and k3.

4. Numerical model

The heat exchanger under consideration is represented in Figure 3A. It is constituted by four tubular heating sections, one holding section, and a number of short curved tubes which are here grouped into three "bends". The liquid product executes counter-flow with respect to super-heated water along the heating sections; the product travels through the holding section and also the bends under thermally-insulated conditions. Figure 3B summarizes how the heat exchanger is represented in the numerical model: a sequence of two-dimensional, axi-symmetrical computational domains. Considering a volume flow rate of 15 L/h, the mean residence time is about 50 seconds.

Table 1 summarizes the boundary conditions assumed for the radial u_r and axial u_z components of the velocity, for the temperature T, and for the swelling degree S. Some of these boundary conditions are closely related to the operating conditions which were specified in running the heat exchanger, namely the volume flow rate ($\dot{V}$), and the temperature at key positions: at the exchanger's inlet (T_1), at the second heating section's outlet (T_2), and at the fourth heating section's outlet (T_3). These three temperatures allowed us to estimate, through global energy budget considerations, the averaged inward heat flux to be applied as boundary condition at the walls of the first and the second heating sections (about 6930 W/m^2) and at

303 the walls of the third and the fourth heating sections (about 4210 W/m^2).

304 Looking for the resolution of equations which govern the coupled phenomena, every
305 computational domain has to be subdivided into a number of small, non-overlapping cells.
306 The rectangular geometry of these domains suggests the adoption of rectangular cells
307 characterized by dimensions *dr* and *dz* along the domain's radius and axis respectively. We
308 chose cells whose length is four times their width (*dz* / *dr* = 4), as a compromise for
309 representing gradients along both directions. Three grids were successively assumed, each of
310 them associated with an increasing number of identical cells in the radial direction: *nr* = 2^5 =
311 32, 2^6 = 64, and 2^7 = 128. For the last grid, we obtain *nz* = 6400 in the case of our heating
312 sections (length 800 mm); considering all the domains required to represent the heat
313 exchanger, the final number is over 4.3 million cells. The mesh resolution corresponding to *nr*
314 = 2^7 is the highest allowed by computer memory capabilities (Intel Xeon CPU X5650 @ 2.67
315 GHz, 64-bits, 32-Gb RAM computer).

316 Governing equations (1, 2, 3, and 7) are solved under steady-state conditions by
317 applying the finite-element method as implemented in the simulation package COMSOL
318 Multiphysics, version 4.4 (Zimmermann, 2006). The solution of the large linear system
319 resulting from the linearization of the coupled equations is reached with the help of the
320 Multifrontal Massively Parallel Sparse Direct Solver (MUMPS; Amestoy et al., 2001, 2006).
321 Satisfactory model convergence was reached after assuming the diffusion coefficient d_S =
322 10^{-8} m^2.s^{-1} in equation (7).

323 Lastly, we are aware that curved tubes situated between two successive heating or
324 holding sections can induce some mixing which tends to homogenize temperature and liquid
325 product properties. Such an influence can be significant, as put in evidence through numerical
326 modeling (Hajmohammadi et al., 2013) as well as analysis of experimental residence time
327 distributions (Ndoye et al., 2012). In developing our numerical model, the curved tubes

("bends") situated between successive heating or holding sections are assumed to play the role of thermally-insulated perfectly-mixed reactors. On the one hand, the mass-weighted value of the product temperature remains unchanged while the fluid parcels travel from the bend's inlet to its outlet. On the other hand, additional transformation is allowed should the product temperature exceed the threshold value Ta = 61.1 °C (see Section 3).

5. Results

Figure 4 presents the main results obtained with the numerical model throughout the heating and the holding sections of the heat exchanger. Grey rectangles indicate the curved tubes (bends) situated between two successive sections. The results were obtained using nr = 2^7 = 128 rectangular cells in the radial direction when building the mesh in all the computational domains.

The temperature field is exhibited in display A. In the heating sections (domains He1, He2, He3, and He4), the starch suspension is warmed from the wall: its temperature increases more rapidly in the vicinity of the wall than at the axis of symmetry.

The starch suspension undergoes progressive transformation should its temperature exceed the threshold value Ta = 61.1 °C. The volume mean diameter and the solid volume fraction are exhibited in displays B and C respectively. In the heating sections, their patterns match the temperature field. In the bends, the product is mixed and subject to additional transformation. Indeed, the fluid leaving the bends is characterized by mass-weighted values of solid volume fraction of 3.58, 5.36, and 8.21 %, which are gradually higher than the values at the outlets of the preceding heating sections: 3.57, 4.82, and 7.63 %, respectively. No transformation occurs in the holding section because it succeeds a bend whose outlet temperature (60.1 °C) is lower than the threshold value Ta.

The apparent viscosity of the starch suspension is shown in display F. At the heat

353 exchanger's inlet, the apparent viscosity is associated with low values (about 0.7 mPa.s) and
354 Newtonian behavior due to the occurrence of untreated starch granules only ($\Phi = \Phi_0$ in
355 equation 10c). Moving forward in the heat exchanger, the apparent viscosity is slightly
356 affected before the onset of starch swelling ($T = Ta$). Beyond this point, the transformation
357 state progresses; as a result, the liquid becomes shear-thinning (the flow behavior index
358 decreases with Φ in equation 10c) while the apparent viscosity values rise (the consistency
359 coefficient increases with Φ in equation 10b). The swelling state is the highest at the wall of
360 the fourth heating section's outlet (domain He4).

361 The apparent viscosity of the starch suspension is here assumed to decrease with
362 temperature following the behavior associated with pure water (equation 10a). The apparent
363 viscosity decreases at the axis of symmetry throughout the two first heating sections (He1 and
364 He2) because the temperature rises under low transformation. Inversely, the temperature's
365 influence on the apparent viscosity can be dominated by that associated with the swelling
366 state when the latter is significant, like in the vicinity of the wall near the outlet of the fourth
367 heating section.

368 The progressive transformation of the starch suspension affects its rheological
369 behavior, which in turn drives the flow field in the heat exchanger. The velocity magnitude
370 and the shear rate predicted by the numerical model are presented in displays D and E. At the
371 heat exchanger's inlet, a fully-developed velocity profile is assumed. In the first heating
372 section (domain He1), the velocity magnitude decreases at the axis from the inlet to the outlet,
373 whereas it increases in the vicinity of the wall; such a result can be related to the apparent
374 viscosity values at the wall, which decrease as a consequence of progressive warming under
375 low product transformation. In the three other heating sections (He2, He3 and He4), on the
376 contrary, the velocity magnitude increases at the axis and decreases near the wall as a
377 consequence of product transformation and increase in apparent viscosity near the wall: fluid

parcels travelling in the vicinity of the wall are slowed down, while those running at the axis undergo acceleration. Such a feature is quite severe in the fourth heating section; relatively high shear rate values are obtained towards its outlet, along a tongue-like region which separates the vicinity of the heating wall (where velocity is vanishing) and the region near the axis (where velocity is the highest).

Figure 5 displays the radial distribution of the volume mean diameter at the outlet of the last heating section (domain He4) as predicted by numerical model simulation after assuming three mesh resolutions. Figure 5A shows results obtained with the highest mesh resolution here considered (nr = 128), while Figure 5B presents the differences between results from a given mesh and those corresponding to nr = 128. Firstly, these differences are often negative (swelling is underestimated); secondly, they become stronger as the mesh becomes coarser; finally, their strongest values occur at about 2.5 mm from the axis, where the radial variation of the volume mean diameter is the highest. These findings can be explained by the progressively-finer representations of the gradients of state variables as the mesh resolution increases.

The influence of mesh resolution can also be assessed in terms of volume mean diameter which corresponds to the mass-weighted value of the solid volume fraction at the outlet of a given section of the heat exchanger. After assuming 32, then 64, and finally 128 cells in the radial direction, the bulk values of the volume mean diameter predicted by the numerical model were respectively of 18.19, 18.26 and 18.30 μm at the outlet of the second heating section, and 25.37, 25.42 and 25.44 μm at the outlet of the fourth heating section. Differences between results corresponding to two successive meshes decrease as the latter become finer, suggesting a convergence-like behavior. We argue that a further leap in mesh resolution, from $nr = 2^7 = 128$ to $nr = 2^8 = 256$, would allow closer results, with differences between respective predictions of the volume mean diameter smaller than 0.05 μm.

Figures 4 and 5 put in evidence that we have satisfactorily solved the coupled problem: while Figure 5 shows that we reached some degree of convergence in solving the equations which govern the relevant phenomena, the two-dimensional fields displayed in Figure 4 are physically consistent. Assessing the performance of model predictions requires comparisons with experimental values. Such a comparison can be performed in terms of mass-weighted values of the swelling state resulting from numerical model simulations.

Experimental results were obtained after running the available heat exchanger under the operating conditions which were applied in numerical modeling simulations (see Table 1). The starch suspension was sampled three times at the outlet of both the second and the fourth heating sections, and immediately cooled down to about 4 °C to avoid additional product transformation. The size distribution analysis of the product samples provided volume mean diameter values of about 16.5 and 31.6 μm respectively after the second and the fourth heating sections, with standard deviations of 0.4 μm. Considering the numerical model simulations which were conducted with the highest mesh resolution allowed, the bulk values for the predicted volume mean diameter after those two heating sections were respectively 18.30 and 25.44 μm (+11 % and –19 % respectively compared to the experimental values).

The level of agreement of numerical coupled modeling with experiment can be compared with that obtained through a simpler modeling approach. The simplest way to characterize the path followed by fluid parcels along a heat exchanger consists in neglecting the radial dependence of both velocity and temperature. In such a one-dimensional model, it is assumed that fluid parcels move according to a plug-flow velocity field, and that they are exposed to a temperature which depends only on the distance from the exchanger inlet. The swelling state of the starch suspension at selected positions of the heat exchanger was estimated through equations (9). For this, the swelling kinetics rate was represented as in the numerical coupled model; in building the thermal history, the bulk temperature was assumed

to vary linearly along the heating sections, and to be constant along the bends and the holding section. At the outlet of the second heating section, the predicted volume mean diameter is identical to the value assumed as boundary condition at the exchanger's inlet; this result is easily understandable because the temperature value at the second heating section's outlet (60.1 °C) is lower than the threshold value Ta = 61.1 °C. Starch swelling takes place along the following sections according to this one-dimensional model; at the outlet of the fourth heating section, the predicted volume mean diameter is 21.5 µm (–32 % compared to the experimental value).

We can summarize that: a) when the suspension bulk temperature does not reach the threshold value *Ta*, the plug-flow and radially-independent temperature approach is unable to predict any starch swelling, contrarily to the numerical coupled model; b) when that threshold is overcome, the simpler approach underestimates the swelling state reached by the starch suspension. Starch swelling can be compared in terms of volume mean diameter value increase between the exchanger's inlet and outlet: we obtain (31.6–16.3) = 15.3 µm from experiment at pilot scale, (25.4–16.3) = 9.1 µm from the numerical coupled model, and (21.5–16.3) = 5.2 µm from the simpler approach. In other words, the numerical model predicts the bulk swelling state of the starch suspension at a level of agreement (–41 % in volume mean diameter increase) which is better than that reached after assuming plug-flow and radially-independent temperature (–66 %).

Finally, a number of reasons can contribute to explain the differences between predictions from the numerical coupled model and respective experimental values. Firstly, the curved tubes (bends) were assumed, in numerical model simulations, to play the role of thermally-insulated perfectly-mixed reactors; actually, we expect the occurrence of slight cooling and incomplete mixing, whose consequences on product transformation are difficult to anticipate. Secondly, starch swelling under heat treatment was assumed to follow a single

453 temperature-dependent swelling kinetics (equation 6), independently on the granule size. The
454 influence of starch granule size on the swelling onset has been scarcely studied (Myllarinen et
455 al., 1998; see references in Sasaki and Matsuta, 1998); however, no generalization seems
456 possible regarding the starch type. On the other hand, we cannot discard some experimental
457 bias in sampling the starch suspension while it flows in the heat exchanger.
458
459 **6. Conclusions and Forthcoming Work**
460
461 Conclusions
462 The key parameters describing the swelling kinetics and the rheological behavior of a
463 starch suspension were estimated from a limited number of experiments at laboratory scale,
464 after studying small volumes of product under heat treatment and continuous agitation. The
465 application of these parameters allowed model predictions of the final swelling state reached
466 by the starch suspension which did agree, to some extent, with observations conducted while
467 running the heat exchanger. We can therefore conclude that kinetics and rheological model
468 parameters can be transferred from laboratory to pilot scale.
469 The plug-flow hypothesis implies no influence of product viscosity on the velocity
470 field, and therefore no coupling between fluid flow, heat transfer and transformation. Such a
471 simpler approach provides worse estimates of the final swelling condition reached by starch
472 granules in suspension, relatively to those obtained with the numerical coupled model. We
473 conclude that the consideration of two-way coupling between the relevant phenomena
474 constitutes a positive improvement in looking for realistic predictions of the product's
475 transformation level.
476
477 Forthcoming work

This study indicates three key issues that deserve attention in implementing numerical coupled models to represent the transformation of realistic food fluid parcels during their pathway in thermal processing units.

Firstly, after representing the heat exchanger under consideration by a sequence of axi-symmetrical two-dimensional (2D) domains, the most obvious following step should be to solve the coupled problem by considering the actual three-dimensional (3D) geometrical characteristics of the equipment. In fact, the thermal mixing due to the secondary flow in curved tubes can be more or less effective depending on the flow rate and the fluid rheological behavior (e.g. Cvetkovski et al., 2015). Inclusion of secondary flow is certainly a positive improvement, and its implementation requires higher computer memory and time resources. The challenging task to solve a similar coupled problem by considering the tubular heat exchanger schematized in Figure 3A is already under way.

Secondly, additional efforts are required in representing the product transformation, as the following step towards more realistic predictions from the numerical model, even in the case of a relatively simple liquid product like a starch suspension. Towards such a goal, experiments were conducted with an optical microscope coupled to a warming plate in order to continuously observe the starch granules' behavior during thermal treatments. Indeed, visual observation of individual granules suggested us that, in the case of modified waxy maize starch, the swelling mechanism presents some stochastic nature while being associated with diffusion of surrounding water into the granule.

Finally, the whole strategy could be adapted to product formulations associated with increasing complexity and industrial relevancy, for instance by studying starch swelling in skim milk and later by adding carrageenan. The notion of swelling degree (associated with starch granules in water) could be replaced by that of "filling degree" associated with all objects floating in the continuous phase. Further attention should be paid to estimating the

503 relevant solid volume fraction. The main structure of the numerical model could be
504 maintained, as the changes would only affect the key parameters describing transformation
505 kinetics and rheological behavior.
506
507 **Acknowledgements:**
508 The research leading to these results received funding from the Carnot Institute Qualiment
509 (INRA, France). We acknowledge Stephan Savarese, Benjamin Loubet and Thierry Gengler
510 (COMSOL France) and Vincent Nicolas (IRSTEA) for fruitful discussions regarding the
511 COMSOL Multiphysics 4.4 software package, as well as Qing Li, Ihssane El Mokhtari, Hela
512 Ferchichi and Emilie Auger (trainees at UMR 1145 GENIAL) for their dedication in helping
513 us conduct experimental and numerical work.
514
515 **References**
516
517 Amestoy, P. R., Duff, I. S., L'Excellent, J.-Y., Koster, J. (2001). A fully asynchronous
518 multifrontal solver using distributed dynamic scheduling. *SIAM Journal of Matrix Analysis*
519 *and Applications*, 23, 15-41.
520
521 Amestoy, P. R., Guermouche, A., L'Excellent, J.-Y., Pralet, S. (2006). Hybrid scheduling for
522 the parallel solution of linear systems. *Parallel Computing*, 32, 136-156.
523
524 Bouvier, L., Moreau, A., Ronse, G., Six, T., Petit, J., Delaplace, G. (2014). A CFD model as a
525 tool to simulate beta-lactoglobulin heat-induced denaturation and aggregation in a plate heat
526 exchanger. *Journal of Food Engineering*, 136, 56-63.
527

528 Chantoiseau, E., Plana-Fattori, A., Doursat, C., Flick, D. (2012). Coupling fluid flow, heat
529 transfer and thermal denaturation-aggregation of beta-lactoglobulin using an Eulerian /
530 Lagrangian approach. *Journal of Food Engineering*, 113, 234-244.
531
532 Cvetkovski, C. G., Reitsma, S., Bolisetti, T., Ting, D. S. K. (2015). Heat transfer in a U-bend
533 pipe: Dean number versus Reynols number. *Sustainable Energy Technologies and*
534 *Assessments (in press).*
535
536 Datta, A. K. (2008). Status of physics-based models in the design of food products, processes,
537 and equipment. *Comprehensive Reviews in Food Science and Food Safety*, 7, 121-129.
538
539 Defraeye, T. (2014). Advanced computational modelling for drying processes - a review.
540 *Applied Energy*, 131, 323-344.
541
542 Doublier, J. L., Durand, S. (2008). A rheological characterization of semi-solid dairy systems.
543 *Food Chemistry*, 108, 1169-1175.
544
545 French, D. (1944). Physical properties of starch. In R. W. Kerr (Ed.), *Chemistry and Industry*
546 *of Starch* (pp. 113-129). Academic Press, New York.
547
548 Galeazzo, F. C. C., Miura, R. Y., Gut, J. A. W., Tadini, C. C. (2006). Experimental and
549 numerical heat transfer in plate heat exchanger. *Chemical Engineering Science*, 61, 7133-
550 7138.
551

552 Hajmohammadi, M. R., Eskandari, H., Saffar-Avval, M., Campo, A. (2013). A new
553 configuration of bend tubes for compound optimization of heat and fluid flow. *Energy*, 62,
554 418-424.
555
556 Huc, D., Matignon, A., Barey, P., Desprairies, M., Mauduit, S., Sieffermann, J. M., Michon,
557 C. (2014). Interactions between modified starch and carrageenan during pasting. *Food*
558 *Hydrocolloids*, 36, 355-361.
559
560 Khatir, Z., Paton, J., Thompson, H., Kapur, N., Toropov, V. (2013). Optimisation of the
561 energy efficiency of bread-baking ovens using a combined experimental and computational
562 approach. *Applied Energy*, 112, 918-927.
563
564 Lagarrigue, S., Alvarez, G., Cuvelier, G., Flick, D. (2008). Swelling kinetics of waxy maize
565 and maize starches at high temperatures and heating rates. *Carbohydrate Polymers*, 73, 148-
566 155.
567
568 Lemus-Mondaca, R. A., Vega-Galvez, A., Moraga, N. O. (2011). Computational simulation
569 and developments applied to food thermal processing. *Food Engineering Reviews*, 3, 121-
570 135.
571
572 Liao, H.-J., Rao, M. A., Datta, A. K. (2000). Role of thermo-rheological behaviour in
573 simulation of continuous sterilization of a starch dispersion. *Transactions of the Institution of*
574 *Chemical Engineers*, 78C, 48-56.
575
576 Liu, H., Xie, F., Yu, L., Chen, L., Li, L. (2009). Thermal processing of starch-based

577 polymers. *Progress in Polymer Science*, 34, 1348-1368.
578
579 Malumba, P., Jacquet, N., Delimme, G., Lefebvre, F., Bera, F. (2013). The swelling behaviour
580 of wheat starch granules during isothermal and non-isothermal treatments. *Journal of Food*
581 *Engineering*, 114, 199-206.
582
583 Matignon, A., Barey, P., Desprairies, M., Mauduit, S., Siefferman, J. M., Michon, C. (2014a).
584 Starch / carrageenan mixed systems: Penetration in, adsorption on or exclusion of carrageenan
585 chains by granules ?. *Food Hydrocolloids*, 35, 597-605.
586
587 Matignon, A., Moulin, G., Barey, P., Desprairies, M., Mauduit, S., Sieffermann, J. M.,
588 Michon, C. (2014b). Starch / carrageenan / milk proteins interactions studied using multiple
589 staining and Confocal Laser Scanning Microscopy. *Carbohydrate Polymers*, 99, 345-355.
590
591 Matignon, A., Neveu, A., Ducept, F., Chantoiseau, E., Barey, P., Mauduit, S., Michon, C.
592 (2015). Influence of thermo-mechanical treatment and skim milk components on the swelling
593 behavior and rheological properties of starch suspensions. *Journal of Food Engineering*, 150,
594 1-8.
595
596 Myllarinen, P., Autio, K., Schulman, A. H., Poutanen, K. (1998). Heat-induced structural
597 changes of small and large barley starch granules. *Journal of the Institute of Brewing*, 104,
598 343-349.
599
600 Nayouf, M., Loisel, C., Doublier, J. L. (2003). Effect of thermomechanical treatment on the
601 rheological properties of crosslinked waxy corn starch. *Journal of Food Engineering*, 59,

209–219.

Ndoye, F. T., Erabit, N., Alvarez, G., Flick, D. (2012). Influence of whey protein aggregation on the residence time distribution in a tubular heat exchanger and a helical holding tube during heat treatment process. *Journal of Food Engineering*, 112, 158-167.

Nicolai, T., Britten, M., Schmitt, C. (2011). Beta-lactoglobulin and WPI aggregates: Formation, structure and applications. *Food Hydrocolloids*, 25, 1945-1962.

Noisuwan, A., Hemar, Y., Wilkinson, B., Bronlund, J. E. (2009). Dynamic rheological and microstructural properties of normal and waxy rice starch gels containing milk protein ingredients. *Starch/Starke*, 61, 214-227.

Norton, T., Sun, D.-W. (2006). Computational fluid dynamics (CFD): An effective and efficient design and analysis tool for the food industry: A review. *Trends in Food Science and Technology*, 17, 600-620.

Norton, T., Tiwari, B., Sun, D.-W. (2013). Computational Fluid Dynamics in the design and analysis of thermal processes: A review of recent advances. *Critical Reviews in Food Science and Nutrition*, 53, 251-275.

Nunez-Santiago, M. C., Tecante, A., Garnier, C., Doublier, J. L. (2011). Rheology and microstructure of kappa-carrageenan under different conformations induced by several concentration of potassium ion. *Food Hydrocolloids*, 25, 32-41.

627 Piculell, L. (2006). Gelling carrageenans. In Stephen, A. M. (Ed.), *Food Polysaccharides and*
628 *their Applications* (pp. 239-287). Taylor & Francis, New York.
629
630 Plana-Fattori, A., Chantoiseau, E., Doursat, C., Flick, D. (2013). An Eulerian-Lagrangian
631 approach for coupling fluid flow, heat transfer, and liquid food product transformation.
632 *Computers and Chemical Engineering*, 52, 286-298.
633
634 Ratnayake, W. S., Jackson, D. S. (2008). Starch gelatinization. *Advances in Food Science and*
635 *Nutrition Research*, 55, 221-268.
636
637 Rocha, K. S. O., Martins, J. H., Martins, M. A., Saraz, J. A. O., Lacerda Filho, A. F. (2013).
638 Three-dimensional modeling and simulation of heat and mass transfer processes in porous
639 media: An application for maize stored in a flat bin. *Drying Technology*, 31, 1099-1106.
640
641 Rodriguez, P., Gonzalez de la Cruz, G. (2003). Photoacoustic measurements of thermal
642 diffusivity of amylose, amylopectin and starch. *Journal of Food Engineering*, 58, 205-209.
643
644 Sasaki, T., Matsuki, J. (1998). Effect of wheat starch structure on swelling power. *Cereal*
645 *Chemistry*, 75, 525-529.
646
647 Schirmer, M., Hochstotter, A., Jeckle, M., Arendt, E., Becker, T. (2013). Physicochemical
648 and morphological characterization of different starches with variable amylose / amylopectin
649 ratio. *Food Hydrocolloids*, 32, 52-63.
650
651 Thomas, D. J., Atwell, W. A. (1999). "Starches". American Association of Cereal Chemists,

St. Paul (Minnesota, USA).

Tolkach, A., Kulozik, U. (2007). Reaction kinetic pathway of reversible and irreversible thermal denaturation of beta-lactoglobulin. *Lait*, 87, 301-315.

Verbeken, D., Bael, K., Thas, O., Dewettinck, K. (2006). Interactions between kappa-carrageenan, milk proteins and modified starch in sterilized dairy desserts. *International Dairy Journal*, 16, 482-488.

Zimmerman, W. B. J. (2006). *Multiphysics Modelling with Finite Element Methods*. World Scientific, Singapore.

Table

Table 1: Boundary conditions taken into account for the radial u_r and axial u_z components of the velocity, for the temperature *T*, and for the swelling degree *S*.

	fluid flow	heat transfer	transformation
inlet (a)(b)(c)	velocity: $u_r = 0,\ u_z\{r\}$	temperature: $T\{r\}$	swelling degree: $S\{r\}$
outlet	null pressure, no viscous stress	convective flux: $\frac{\partial T}{\partial z} = 0$	convective flux: $\frac{\partial S}{\partial z} = 0$
axis	symmetry: $u_r = 0,\ \frac{\partial u_z}{\partial r} = 0$	symmetry: $\frac{\partial T}{\partial r} = 0$	symmetry: $\frac{\partial S}{\partial r} = 0$
wall	no slipping: $u_r = u_z = 0$	flux density (d)(e)	no diffusion: $\frac{\partial S}{\partial r} = 0$

(a) first heating section: the suspension is assumed to be at the temperature T_1 = 43.9 °C, containing untreated starch granules only (S = 0); the axial velocity follows the fully-developed parabolic profile associated with the volume flow rate $\dot{V}$ = 15 L/h (mean velocity $\overline{u}_z$ = 0.083 m.s^{-1}, Reynolds number of about 1040).

(b) other sections, when the preceding one is not a bend: the temperature, the swelling degree and the axial velocity follow the distributions $T\{r\}$, $S\{r\}$ and $u_z\{r\}$, which were predicted at the outlet of the preceding section.

(c) other sections, when the preceding one is a bend: the temperature assumes its mass-weighted (bulk) value $\widetilde{T}$ at the bend's outlet; the swelling degree assumes the value $\widetilde{S}$ which corresponds to the mass-weighted value $\widetilde{\Phi}$ of the solid volume fraction at the bend's outlet; the axial velocity follows $u_z\{r\} = \overline{u}_z \left(\frac{3\widetilde{n}+1}{\widetilde{n}+1}\right)\left(1-\frac{r}{R}\right)^{\frac{(\widetilde{n}+1)}{\widetilde{n}}}$ where $\widetilde{n}$ is the flow behavior index given through equation (10c) by replacing $\Phi = \widetilde{\Phi}$.

(d) heating and holding sections: inward heat flux estimated from the section's global energy budget, by taking into account the temperatures T_1 = 43.9 °C at the exchanger's inlet, T_2 = 60.1 °C at the second heating section's outlet, and T_3 = 70.0 °C at the fourth heating section's inlet.

(e) bends: thermal insulation.

Figure Captions

Figure 1: Key results regarding the evolution of the starch suspension under thermal treatments: A) the sample thermal history; B) the mean volume diameter as function of the heating time, obtained from experiment and estimated through the second-order kinetics; C) predicted versus experimental values for the mean volume diameter.

Figure 2: Apparent viscosity values at 20 °C of the starch suspension, after selected thermal treatments. Lines indicate the corresponding predictions of apparent viscosity as a function of shear rate and solid volume fraction.

Figure 3: Three-dimensional (A) and two-dimensional axi-symmetrical (B) schematic representations of the heat exchanger under consideration. The heating sections are indicated in red, the curved tubes (bends) in blue, and the holding section in green. In scheme B, the dashed line and the red continuous lines indicate the axis of symmetry and the heating walls, respectively.

Figure 4: Numerical model predictions for the temperature, the mean volume diameter and the volume fraction associated with starch granules, the velocity magnitude, the shear rate, and the apparent viscosity throughout the heating and holding sections of the heat exchanger.

Figure 5: Mean volume diameter as predicted by the numerical model at the outlet of the fourth heating section: A) results obtained by assuming a mesh consisting of 128 rectangles in the radial direction; B) difference between results obtained by assuming successively 64, and 32 rectangles in the radial direction, and results shown in the display A.

Figure

A

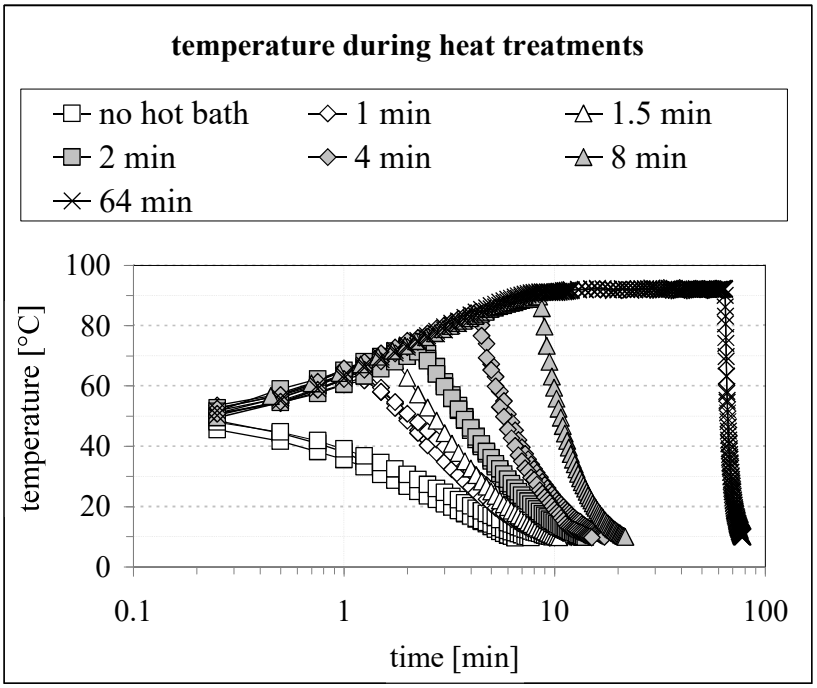
temperature during heat treatments
no hot bath
1 min
1.5 min
2 min
4 min
8 min
64 min
temperature [°C]
100
80
60
40
20
0
0.1
1
10
100
time [min]

B

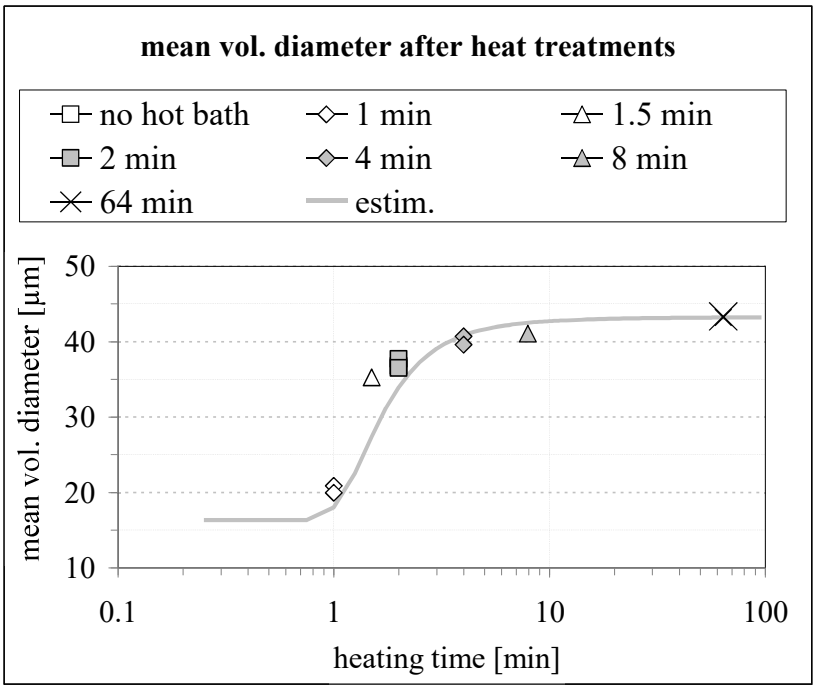
mean vol. diameter after heat treatments
no hot bath
1 min
1.5 min
2 min
4 min
8 min
64 min
estim.
mean vol. diameter [µm]
50
40
30
20
10
0.1
1
10
100
heating time [min]

C

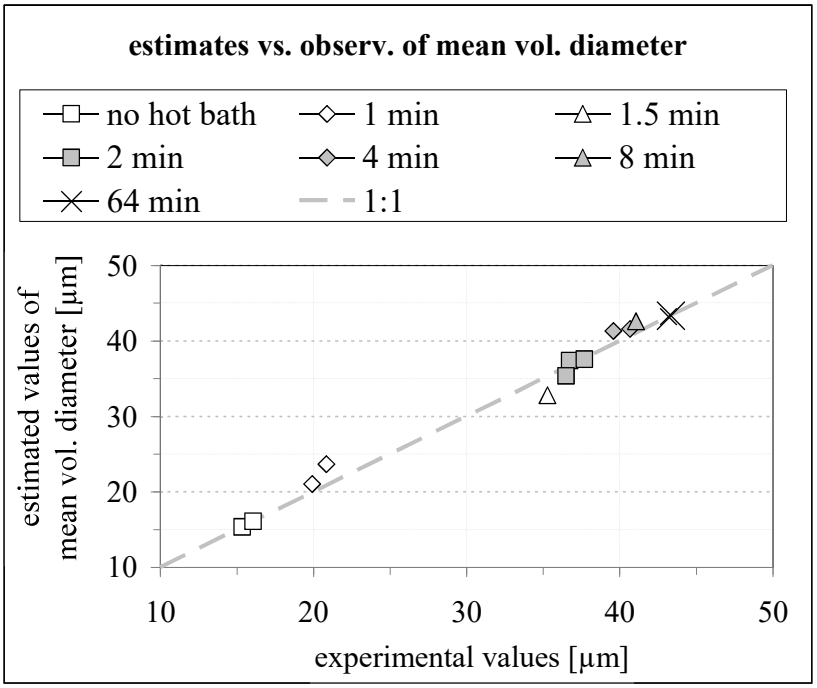
estimates vs. observ. of mean vol. diameter
no hot bath
1 min
1.5 min
2 min
4 min
8 min
64 min
1:1
estimated values of mean vol. diameter [µm]
50
40
30
20
10
10
20
30
40
50
experimental values [µm]

Figure

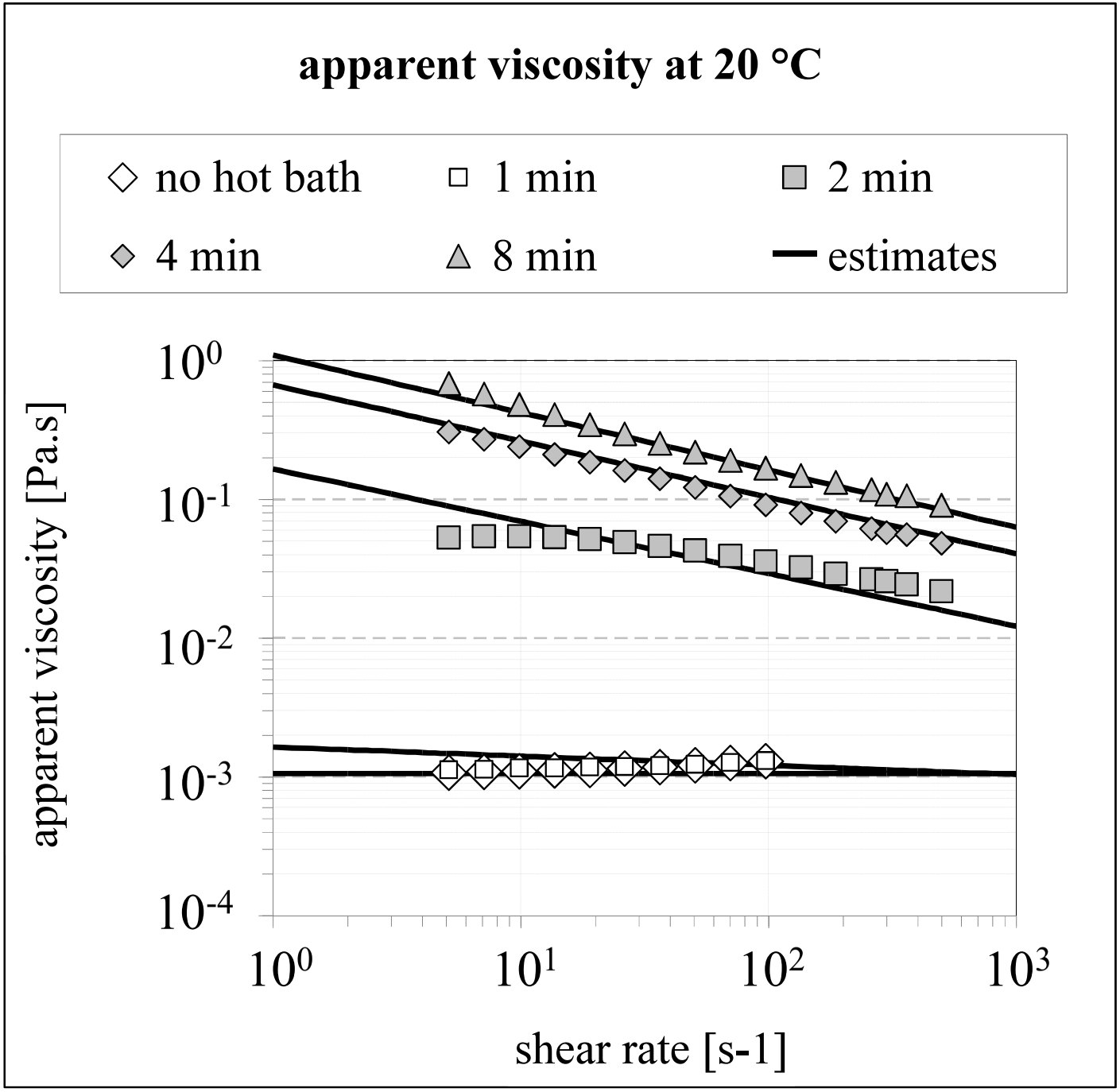
apparent viscosity at 20 °C
no hot bath
1 min
2 min
4 min
8 min
estimates
apparent viscosity [Pa.s]
10^0
10^-1
10^-2
10^-3
10^-4
10^0
10^1
10^2
10^3
shear rate [s-1]

Figure

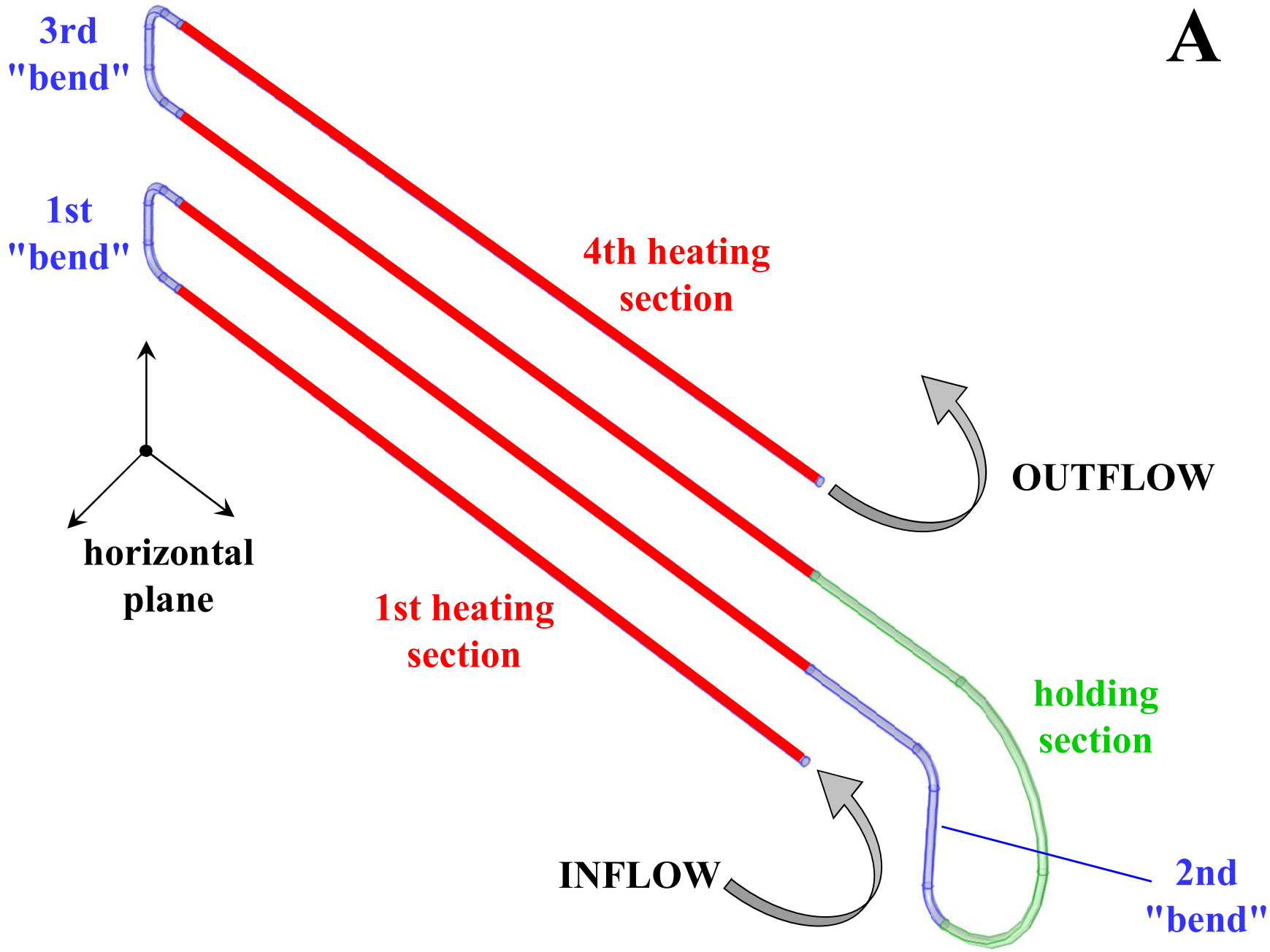
A
3rd
"bend"
1st
"bend"
4th heating
section
OUTFLOW
horizontal
plane
1st heating
section
holding
section
INFLOW
2nd
"bend"

Figure

B

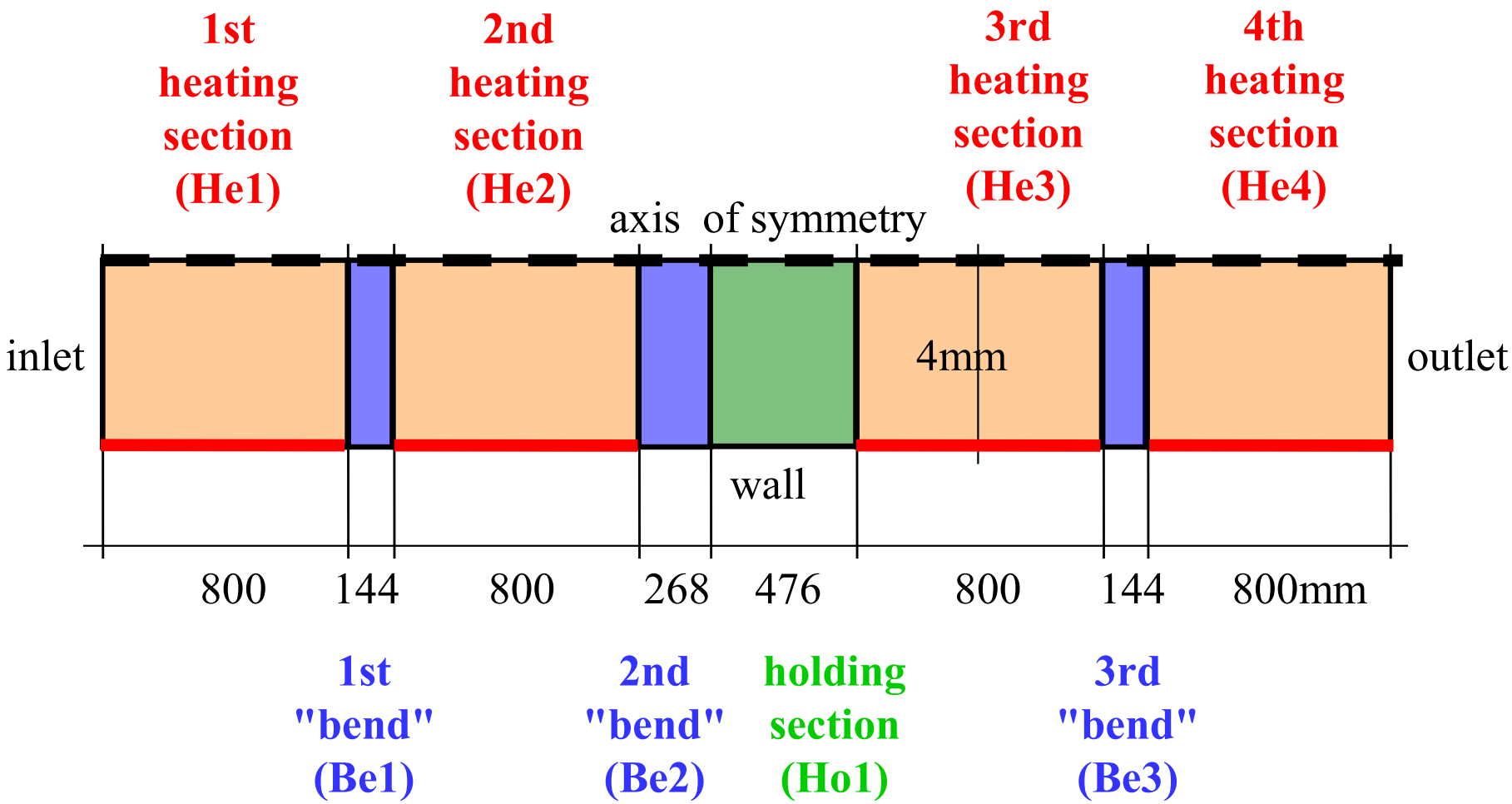
1st heating section (He1)
2nd heating section (He2)
3rd heating section (He3)
4th heating section (He4)
axis of symmetry
inlet
outlet
4mm
wall
800
144
800
268
476
800
144
800mm
1st "bend" (Be1)
2nd "bend" (Be2)
holding section (Ho1)
3rd "bend" (Be3)

Figure

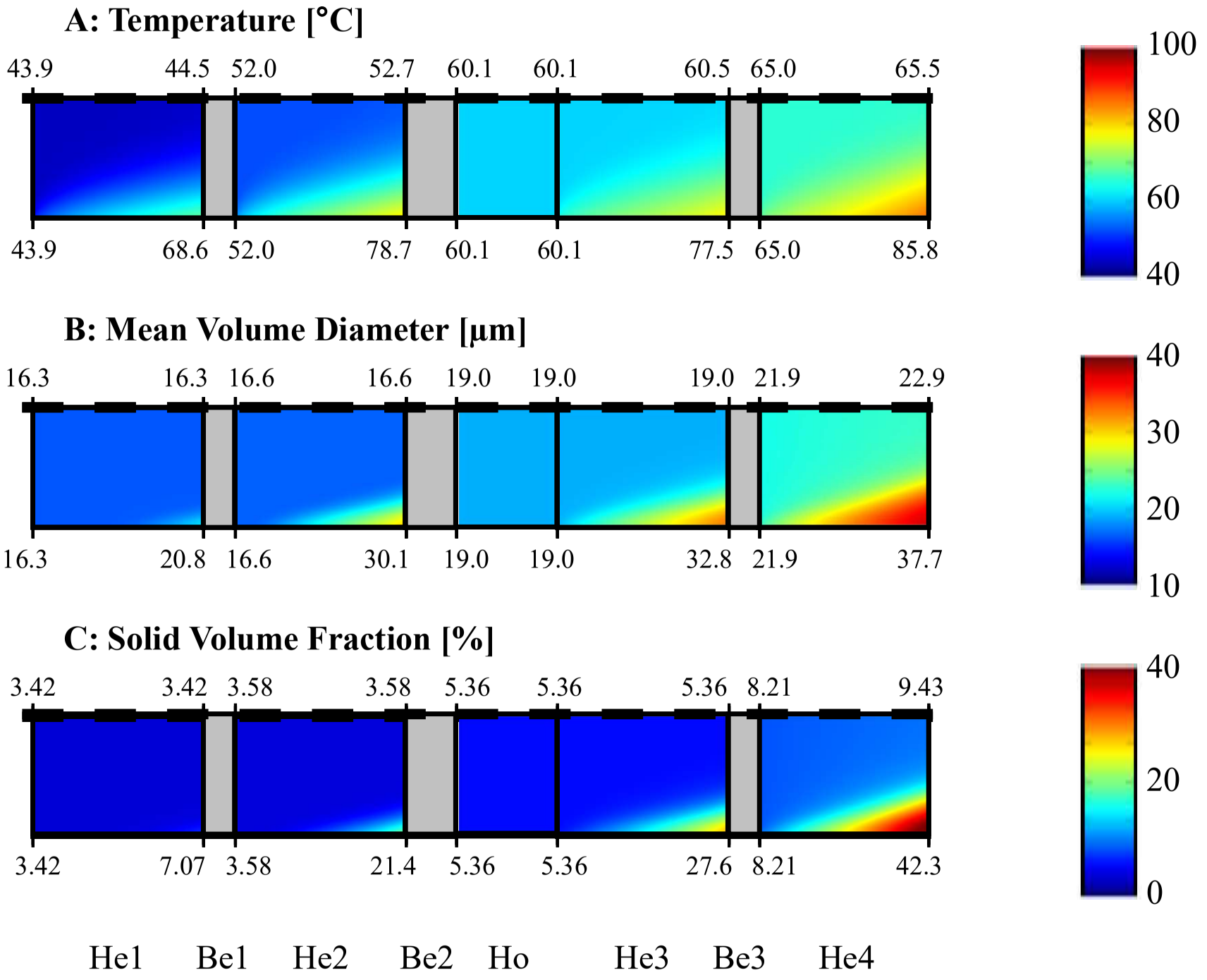
A: Temperature [°C]
43.9 44.5 52.0 52.7 60.1 60.1 60.5 65.0 65.5
43.9 68.6 52.0 78.7 60.1 60.1 77.5 65.0 85.8
100
80
60
40
B: Mean Volume Diameter [µm]
16.3 16.3 16.6 16.6 19.0 19.0 19.0 21.9 22.9
16.3 20.8 16.6 30.1 19.0 19.0 32.8 21.9 37.7
40
30
20
10
C: Solid Volume Fraction [%]
3.42 3.42 3.58 3.58 5.36 5.36 5.36 8.21 9.43
3.42 7.07 3.58 21.4 5.36 5.36 27.6 8.21 42.3
40
20
0
He1 Be1 He2 Be2 Ho He3 Be3 He4

Figure

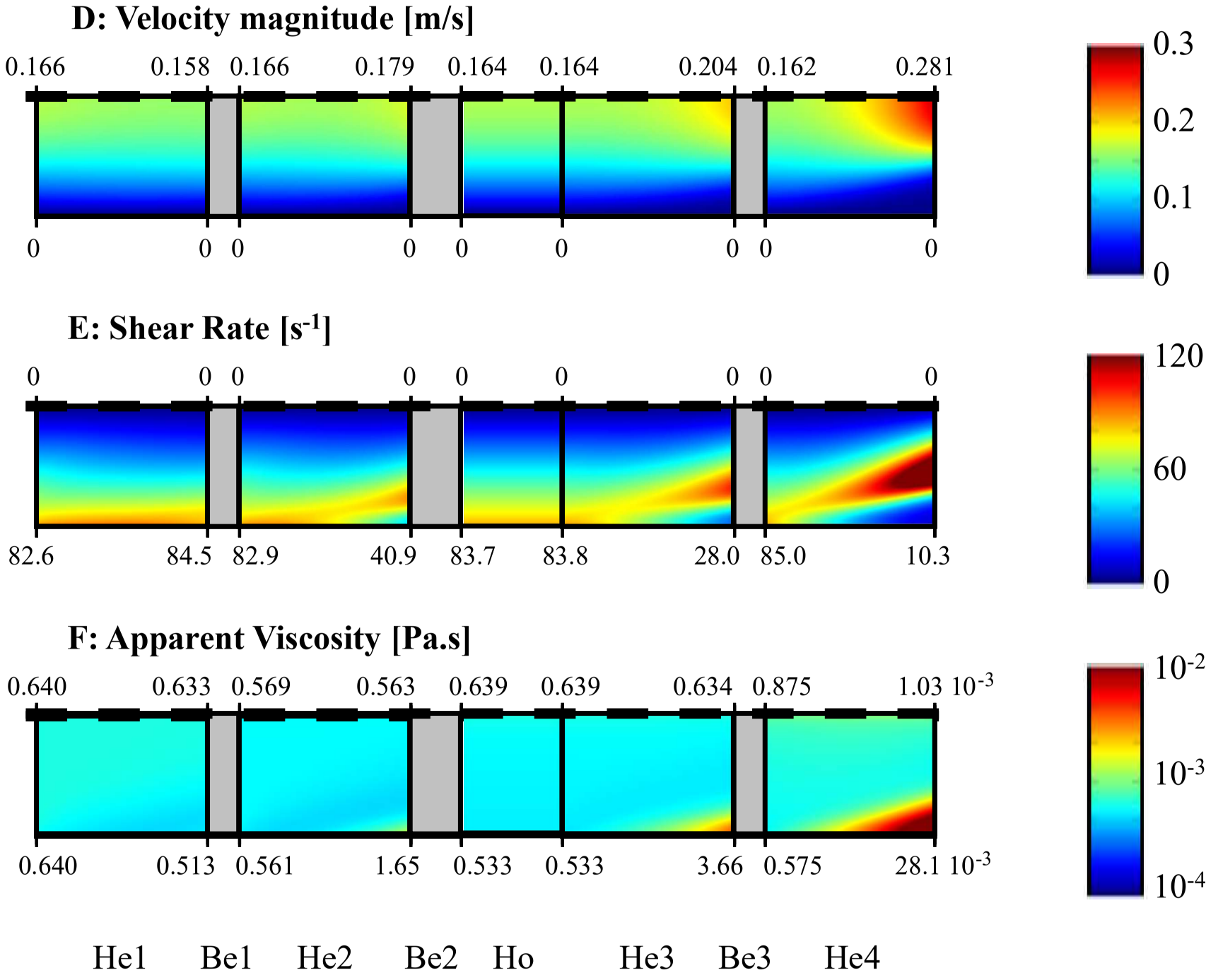
D: Velocity magnitude [m/s]
0.166 0.158 0.166 0.179 0.164 0.164 0.204 0.162 0.281
0 0 0 0 0 0 0 0 0
0.3
0.2
0.1
0
E: Shear Rate [s-1]
0 0 0 0 0 0 0 0 0
82.6 84.5 82.9 40.9 83.7 83.8 28.0 85.0 10.3
120
60
0
F: Apparent Viscosity [Pa.s]
0.640 0.633 0.569 0.563 0.639 0.639 0.634 0.875 1.03 10-3
0.640 0.513 0.561 1.65 0.533 0.533 3.66 0.575 28.1 10-3
10-2
10-3
10-4
He1 Be1 He2 Be2 Ho He3 Be3 He4

Figure

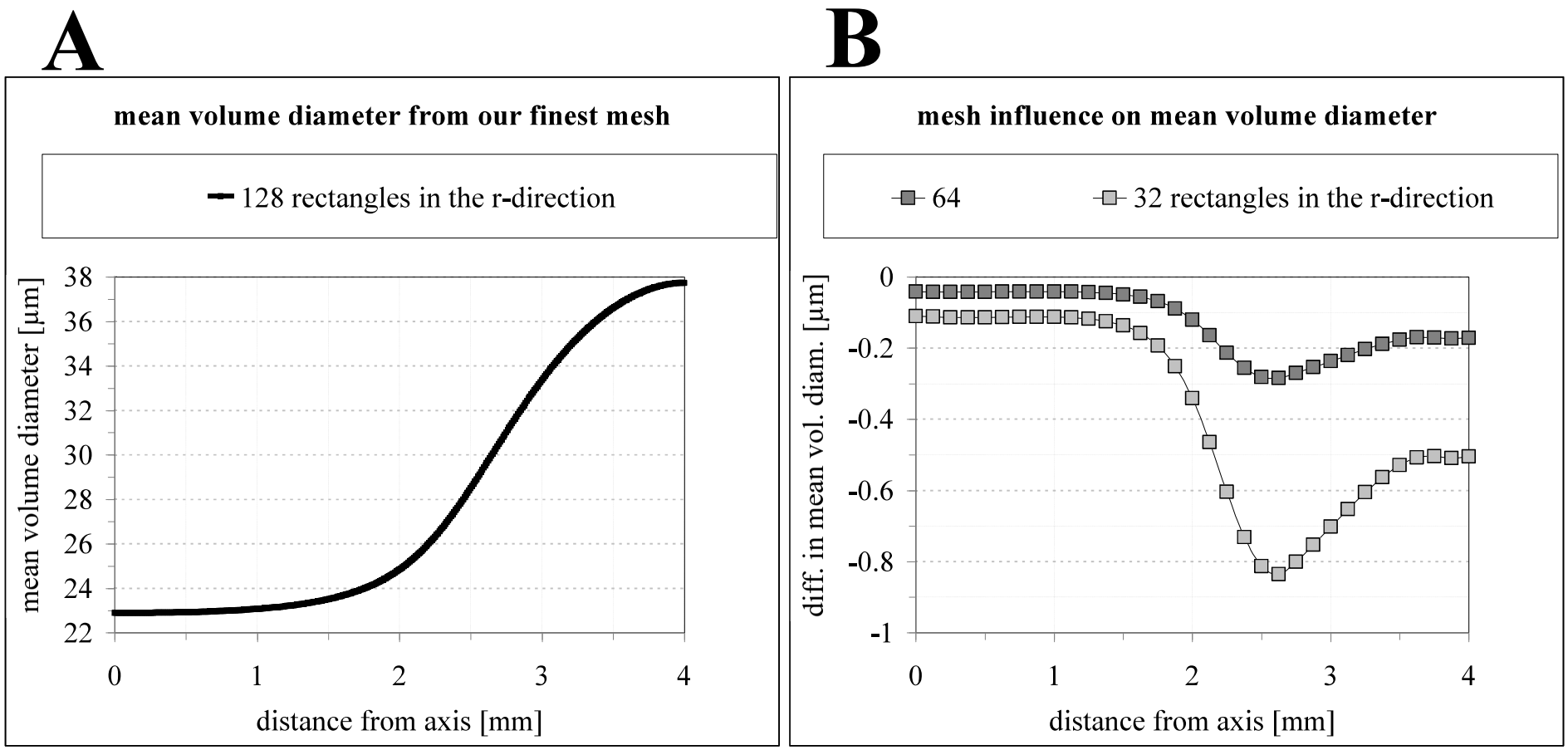
A
mean volume diameter from our finest mesh
128 rectangles in the r-direction
mean volume diameter [µm]
38
36
34
32
30
28
26
24
22
0
1
2
3
4
distance from axis [mm]
B
mesh influence on mean volume diameter
64
32 rectangles in the r-direction
diff. in mean vol. diam. [µm]
0
-0.2
-0.4
-0.6
-0.8
-1
0
1
2
3
4
distance from axis [mm]

Table

Table 1: Boundary conditions taken into account for the radial u_r and axial u_z components of the velocity, for the temperature *T*, and for the swelling degree *S*.

	fluid flow	heat transfer	transformation
inlet (a)(b)(c)	velocity: $u_r = 0,\ u_z\{r\}$	temperature: $T\{r\}$	swelling degree: $S\{r\}$
outlet	null pressure, no viscous stress	convective flux: $\frac{\partial T}{\partial z} = 0$	convective flux: $\frac{\partial S}{\partial z} = 0$
axis	symmetry: $u_r = 0,\ \frac{\partial u_z}{\partial r} = 0$	symmetry: $\frac{\partial T}{\partial r} = 0$	symmetry: $\frac{\partial S}{\partial r} = 0$
wall	no slipping: $u_r = u_z = 0$	flux density (d)(e)	no diffusion: $\frac{\partial S}{\partial r} = 0$

(a) first heating section: the suspension is assumed to be at the temperature T_1 = 43.9 °C, containing untreated starch granules only (S = 0); the axial velocity follows the fully-developed parabolic profile associated with the volume flow rate $\dot{V}$ = 15 L/h (mean velocity $\overline{u}_z$ = 0.083 m.s^{-1}, Reynolds number of about 1040).

(b) other sections, when the preceding one is not a bend: the temperature, the swelling degree and the axial velocity follow the distributions $T\{r\}$, $S\{r\}$ and $u_z\{r\}$, which were predicted at the outlet of the preceding section.

(c) other sections, when the preceding one is a bend: the temperature assumes its mass-weighted (bulk) value $\widetilde{T}$ at the bend's outlet; the swelling degree assumes the value $\widetilde{S}$ which corresponds to the mass-weighted value $\widetilde{\Phi}$ of the solid volume fraction at the bend's outlet; the axial velocity follows $u_z\{r\} = \overline{u}_z \left(\frac{3\widetilde{n}+1}{\widetilde{n}+1}\right)\left(1-\frac{r}{R}\right)^{\frac{(\widetilde{n}+1)}{\widetilde{n}}}$ where $\widetilde{n}$ is the flow behavior index given through equation (10c) by replacing $\Phi = \widetilde{\Phi}$.

(d) heating and holding sections: inward heat flux estimated from the section's global energy budget, by taking into account the temperatures T_1 = 43.9 °C at the exchanger's inlet, T_2 = 60.1 °C at the second heating section's outlet, and T_3 = 70.0 °C at the fourth heating section's inlet.

(e) bends: thermal insulation.